Checklist for the use of potassium concentrations in siliciclastic sediments as paleoenvironmental archives

T. Matys Grygar, K. Mach, Mathieu Martínez

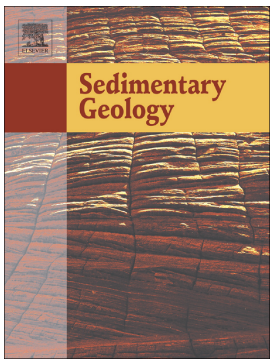

Checklist for the use of potassium concentrations in siliciclastic sediments as paleoenvironmental archives

T. Matys Grygar, K. Mach, M. Martinez

PII: S0037-0738(19)30021-1
DOI: https://doi.org/10.1016/j.sedgeo.2019.01.010
Reference: SEDGEO 5442

To appear in: *Sedimentary Geology*

Received date: 30 October 2018
Revised date: 28 January 2019
Accepted date: 29 January 2019

Please cite this article as: T.M. Grygar, K. Mach and M. Martinez, Checklist for the use of potassium concentrations in siliciclastic sediments as paleoenvironmental archives, Sedimentary Geology, https://doi.org/10.1016/j.sedgeo.2019.01.010

Checklist for the use of potassium concentrations in siliciclastic sediments as paleoenvironmental archives

T. Matys Grygar [a,*], K. Mach [b], M. Martinez [c]

[a] Institute of Inorganic Chemistry, AS CR, v.v.i., 250 68 Řež, Czech Republic, grygar@iic.cas.cz

[b] North Bohemian Mines, j.s.c., 5. května 2013, 418 01, Bílina, the Czech Republic, mach@sdas.cz

[c] Univ Rennes, CNRS, Géosciences Rennes, UMR 6118, 35000 Rennes, France, mathieu.martinez@univ-rennes1.fr

* corresponding author

Abstract

Weathering indices quantify the release of mobile elements from source units of soils and sediments. They have been employed in geosciences for more than three decades, but their performance in sedimentary archives can still be improved by deciphering other forcing factors than climatic. From the most common alkali and alkaline earth metals included in the weathering indices, K seems to be most suitable for deciphering paleoclimate records of temperate to subtropical non-arid climates, assuming the interpretation respects the complex of controlling factors on sediment geochemistry. As a case study, normalised K concentrations in siliciclastic sediments of the Most Basin (Miocene period, central Europe) are revisited here and variations compared with modern fluvially transported solids. Existing knowledge on manifold controls of K concentrations in sediments is summarised and used to propose list of possible controlling factors, in particular Al/Si and Zr/Rb as grain-size proxies, Ti/Al as provenance proxy relevant for K concentration in parent rocks,

and K/Rb as a measure for possible effects of metasomatism. The K/Al or K/Ti element ratios may be efficient in chemostratigraphic correlations in siliciclastic basins and efficient proxies for chemical weathering in the source area. The proposals in this work should stimulate future studies to overcome the underrepresentation of continental sediments in paleoclimate reconstructions.

Keywords stratigraphy; chemostratigraphy; major elements; lake sediments; potassium; past climate

1. Introduction

Most climate reconstructions of the Cenozoic period are based on marine sediments with major biogenic components (Zachos et al., 2001; De Vleeschouver et al., 2017; Miller et al., 2017), while continental siliciclastic (detrital) sedimentary archives have been used less frequently (Abels et al., 2010; 2013, Valero et al., 2014, 2017, Sun et al., 2015). Currently, continental archives seem underrepresented in climate reconstructions, although they could overcome a problem like a widespread hiatus in marine sediments from the periods tightly preceding the Miocene Climatic Optimum (MCO) (Miller et al., 2017), which hinders correlation of existing sedimentary records, dating of the MCO triggers, and their identification. The continental archives of the MCO are, however, rare (Matys Grygar et al., 2014, 2017b; Sun et al., 2015). The use of normalised K concentrations in fine siliciclastic sediments represent an opportunity for broader future use of continental sediments.

The variations in K in the sediment profiles may be governed by several mechanisms. In sediments with substantial contribution of biogenic components, raw K concentration, ^{40}K gamma activity (Baumgarten et al., 2015), or K concentrations relative to Ca or Si (i.e., geochemically normalised K concentrations) may be robust proxies for the variable proportion of detrital and autochthonous components (Abels et al., 2005; Stockhecke et al., 2014; Kwiecien et al., 2015). There are cases where the proportions of detrital and biogenic components based on K variations were climatically controlled and exhibited orbital forcing (Abels et al., 2005; Baumgarten et al., 2015). Variations in K concentrations in the detrital components may, however, bear even subtler information.

In predominantly siliciclastic sediments, the K concentrations may be controlled by chemical weathering intensity in the sediment source area, with weathering products being progressively depleted in K (Gaillardet et al., 1999). In traditional chemical weathering proxies, such as Chemical Index of Alteration (CIA) introduced in 1980s (weathering proxies have recently been overviewed by Guo et al., 2018), the release of a sum of certain mobile

ions (Na, K, Mg, and Ca) from solids is quantified by their proportion to immobile elements. Gaillardet et al. (1999) introduced weathering (mobility) indices α as the ratios of a single mobile element (Mg, Ca, Na, Sr, K, and Ba) to a specific non-mobile element with similar magmatic compatibility (Al, Ti, Sm, Nd, Th, and Th, respectively) in the sample and the upper continental crust (UCC). Garzanti et al. (2013) modified that original definition by choosing Al as a normalising element for all mobile ions, as Al is more suitable for grain-size correction than elements present mainly in heavy minerals. The modified α index for K is the ratio of Al/K in the examined sediment according to Garzanti et al. (2013) thus is:

$\alpha^{Al}K = (Al/K)/(Al/K)_{UCC}$

Among the mobile cations, Mg and in particular Ca are too readily incorporated in autochthonous and diagenetic carbonates, which can blur or overwrite the original weathering signature in the clastic components. These carbonates may be removed by acid leaching before the analysis that is tiresome and might be a problem for more stable carbonates such as siderite and less stable detrital components such as smectite. In contrast, Na is too easily released by chemical weathering and thus its concentration in mature sediments is mainly grain-size controlled (it is only present in coarser particles of primary minerals, Bouchez et al., 2011; von Eynatten et al., 2016). The concentration of the less mobile K, usually in geochemically normalised form such as the K/Al ratio, could thus provide the most straightforward weathering proxy under temperate to warm climates, as it was demonstrated for marine sediments deposited close to river estuaries (Clift et al., 2014; Zhao et al., 2018), continental foreland basins (Vögeli et al., 2017), continental basins in semiarid climates (Foerster et al., 2015, 2018), and freshwater lakes (Matys Grygar et al., 2014, 2017a, 2017b). The K concentrations in sediment profiles, covering sufficiently long time interval, may exhibit orbital signatures, which prove their climatic control (Colin et al., 2014; Foerster et al., 2015, 2018; Matys Grygar et al., 2014, 2017a, 2017b, 2019).

Why has K-chemostratigraphy not yet been added to a conventional arsenal of paleoclimate proxies for continental settings? The reason is in the overlap of factors controlling K concentration in sediments. (1) The geochemical composition of mature sediment is mainly driven by the interplay between sediment grain size (sorting) and provenance (Fralick and Kronberg, 1997; Bouchez et al., 2011; Garzanti et al., 2011; Tanaka and Watanabe, 2015; Garzanti and Resentini, 2016; von Eynatten et al., 2016; Zhao et al., 2018). Their correct handling is not trivial and needs further research and testing. (2) In hydrologically closed lacustrine or palustrine environments, the main mechanism controlling K concentrations may be the neo-formation of K-carriers in sediments in contact with pore waters mineralised during prolonged droughts (Foerster et al., 2015), in particular formation of analcime, illite, and feldspars from dissolved K^+, kaolinite and other clay minerals (Larsen, 2008; Kříbek et al., 2017; Foerster et al., 2018). This mechanism is thermodynamically analogous to "retrograde" clay mineral formation in the marine environment (Cuadros et al., 2017) and basinal brines (van den Kamp, 2016). (3) Fine (clayey) siliciclastic sediments may undergo K-metasomatism, either in basinal brines rich in K^+, or in closed systems in which fine clastic deposits alternate with arkosic beds and are subjected to K^+ migration and retrograde reactions in the circulating pore water (van den Kamp, 2016). All those controlling factors might be perceived as creating a too complex interplay which makes the interpretation of K concentrations in terms of past climate equivocal.

Geochemistry offers several inter-element relationships that could reveal possible non-climatic controls of K concentrations (e.g., Bouchez et al., 2011; van den Kamp, 2016; Xu et al., 2018; Zhao et al., 2018). The aim of this paper is to outline how to evaluate the element-controlling factors driving K concentrations in sedimentary archives to isolate desired paleoclimatic signals. Our work is based on comparison of chemical composition of lacustrine sediments of the Most Basin (the Czech Republic, Miocene age, Fig. 1). with

modern fluvial sediments, discussion of the grain-size control on sediment composition, and evaluation of possible risks in the K-concentration use in sedimentary archives. We propose a checklist of factors, which could facilitate broader use of normalised K concentrations in paleoenvironmental and stratigraphic studies in the continental realm.

2. Settings

This paper revisits the geochemical composition of the Most Basin lacustrine deposits, on which details were published by Matys Grygar and Mach (2013) and Matys Grygar et al. (2014, 2017a, 2017b). The Most Basin (Fig. 1), a part of the Ohře Rift, was denoted as an incipient rift by Rajchl et al. (2009). The Ohře Rift (also referred to as the Eger Graben, Eger Rift, or Ohře Graben) was developed within the European Cenozoic Rift System (Dèzes et al., 2004; Ulrych et al., 2011) as a part of the Alpine orogenesis. Its Early Miocene subsidence was nonetheless not coeval with tectonic movement in other basins in that rift system (Ulrych et al., 2011). Fine sediments addressed in this paper originated from the central and NW part of a half-graben structure with the preserved area of 873 km^2. The Most Basin catchment was subjected to humid temperate climate with mean annual precipitation of 800-1300 mm, mean annual temperature 14-19 °C, and the coldest month with mean temperature around the freezing point (Teodoridis and Kvaček, 2015), i.e., by ca. 10 °C warmer and by ca. 50 % higher precipitation than today. It promoted intense chemical weathering in the basin source areas. The Most Basin paleolake was hydrologically open (overfilled). The sediments studied here thus do not contain chemogenic components typical for hardwater lakes or palustrine environment, in contrast to the neighbouring Cheb-Sokolov Basin within the same graben, which has abundant calcium carbonates and gypsum and neo-formed K-bearing minerals (Kříbek et al., 2017).

The lacustrine siliciclastic deposits of the Most Basin (Libkovice, Lom, and Osek members) are monotonous grey silty clays with no lithological changes apparent under visual

examination. That uniformity hampered a definition of stratigraphic units in the Most Basin during more than half century of intense coal prospections in the Czech Republic. The Most Basin deposits are distinct from deposits of ephemeral lakes, such as those in Mediterranean Cenozoic basins or other heterogeneous sequences with facies alteration that might partly result from autogenic cycles (discussion in Alonso-Zarza et al., 2012) or diagenesis (discussion in Martínez-Braceras et al., 2017). The Most Basin sediments are thus suitable for a study of the element relationships in siliciclastic sediments. Geochemically normalised K concentrations in the Most Basin lacustrine sediments (K/Ti or K/Al ratios) have indeed provided robust stratigraphic correlations at a basin scale (Matys Grygar and Mach, 2013; Matys Grygar et al., 2017a, 2017b). Normalised K variations in the Libkovice Member exhibit orbital control, which together with magnetic polarity analysis produced an age model for the studied lacustrine sequence (Matys Grygar et al., 2014, 2017b, 2019). Geochemical analysis allowed defining criteria to distinguish local stratigraphic units (Fig. 2), of which spatial distribution and lithological features are consistent with the development of the Most Basin after the end of the main coal seam formation (Mach et al., 2014).

The source area of the Most Basin sediments included crystalline and sedimentary rocks from an extensive catchment south of the basin (Mach et al., 2014), with a certain contribution from remnants of outcropping Oligocene mafic lavas (Ulrych et al., 2002) formed mainly in the pre-rift and early rift phases (Rajchl et al., 2009; Ulrych et al., 2011).

3. Methods and datasets

The Most Basin sediments were sampled from drill cores, dried under ambient conditions, ground in a planetary mill (Pulverisette, Fritsch), and analysed by energy dispersive X-ray fluorescence (XRF) spectrometers MiniPAL4 or Epsilon 3^X (PANalytical), as described by Matys Grygar et al. (2014, 2017a, 2017b). Spectra acquisition was optimised to obtain reliable signals also for light elements, such as Al and Si. Calibration was performed using

certified reference materials (NIST numbers 1646a, 2702, 2704, and 2711a by NIST, USA, CTA FFA-1 by Institute of Nuclear Chemistry and Technology, Warsaw, Poland, and Metranal numbers 31 and 34 by Analytika, Prague, Czech Republic). The samples were analysed as loose powders, which may produce textural effects on the analytical signals. Similarly, as in XRF analysis by core scanners, expression of the results as element ratios decreases such texture effects and noise (Abels et al., 2005; Hennekam and de Lange, 2012; Wilhelms-Dick et al., 2012; Colin et al., 2014).

Compositional datasets HK591 core were already used in previous papers (Matys Grygar et al., 2014, 2017a, 2017b) while DO565 and LB432 cores were analysed newly. In this work, we evaluate the geochemical mechanisms behind variations in their K concentration in a generally applicable manner. The Most Basin data processing is supported by comparison with datasets on recent sediments published by other authors, in particular the composition of current solids transported by the Amazon River (Bouchez et al., 2011) and by the Ganga-Brahmaputra river system (Garzanti et al., 2011). Sediment, bedload, and suspended load of those modern rivers are evaluated jointly. The quoted recent river systems carry sediments from sufficiently large catchments to level possible local geochemical anomalies. They can thus be considered to represent the upper continental crust subjected to chemical weathering and then to repeated fluvial sorting.

Spectral analysis (identification of orbital signatures) was performed as described by Matys Grygar et al. (2017a, 2017b, 2019). The long-term trends were removed from the data to make the mean and the variance of the analysed signal stationary. The spectral analyses were then performed on the detrended data using the multi-taper method, using three 2π-tapers (Thomson, 1982, 1990). The confidence levels were then calculated using the LOWSPEC method (Meyers, 2012). The method first consists in pre-whitening the analysed series by removing the red-noise background from the time series. Then, a new spectral back-ground is fitted to the pre-whitened spectrum and the confidence levels are

extrapolated assuming a chi-squared distribution. Taner filters were then used to isolate frequency bands of interest in the spectra (Taner, 2003).

4. Results and discussion

4.1 Inter-element relationships in Most Basin sediments

Grain-size proxies are necessary for evaluation of the Most Basin sediments because their direct granulometric analysis is prevented by their compaction and the presence of >5 % siderite. We preferred not to remove siderite and organic matter by chemical leaching because this treatment could damage the finest clay minerals, such as smectites abundant in the Most Basin deposits.

The interrelation of Al/Si and Zr/Rb ratios, two grain-size proxies broadly applicable to fine sediments (Chen et al., 2006; Bouchez et al., 2011; Guo et al., 2018; Xu et al., 2018) is shown in Fig. 3. The Most Basin compositions plot similarly in Fig. 3B as reference datasets that shows broad applicability of those proxies for mature sediments. Zr/Rb is much larger in coarser (silty) sediments, while in (clayey) finer deposits, this ratio decreases below that in the UCC, because most Zr in sediments is carried by zircons ($ZrSiO_4$), whose crystal size belongs typically to coarse silt-finest sand size fractions (Fralick and Kronberg, 1997; Gärtner et al., 2013). The distribution of Rb, as well as K, in grain-size fractions depends on sediment maturity. Both elements are nearly equally distributed in all grain sizes in immature sediments (von Eynatten et al., 2016; Matys Grygar et al., 2018), but in mature sediments, both elements are carried mainly by clay minerals in the finest fraction. The steep increase in Zr/Rb towards coarser particles (Fig. 3, note logarithmic scale in y-axis) is typical for mature sediments mostly composed of silt and clay with negligible Rb carried by coarser particles. Fig. 3B proves the major grain-size control on Al, Si, Rb, and Zr, with no

"unsupported" elements such as autochthonous (e.g., biogenic) silica, which would have plot left of the major groups of points in Fig. 3B.

The major controls over Al and Si concentrations in the Most Basin are shown in Al vs. Si scatter plot in Fig. 4A. The autochthonous components in the Most Basin sediments, such as siderite in lacustrine clays or organic matter in coaly clays, "dilute" equally Al and Si and thus shift their compositional data towards the origin point (0,0) in Fig. 4A. When the percentage of siderite is subtracted from the composition, the Al and Si concentrations in the remaining (carbonate-free) portion of the sediments are mainly controlled by the quartz content and clay assemblage (Fig. 4B). Al/Si ratio decreases in the order of quartz < K-feldspar < illite < smectite < kaolinite. The comparison shows that Al/Si will not only act as a grain-size proxy but will also reflect Al/Si ratios in individual clay minerals. This effect will inevitably be more prominent in the finest sediments with a low quartz concentration. Nevertheless, Al is probably the best proxy for the content of finest size fractions in mature siliciclastic sediments.

The dependence of Ti/Al on Al/Si in the Most Basin sediments is shown in Fig. 5A. Ti/Al shows similar grain-size control in all examined datasets, including reference ones (Fig. 5B). Although both Al and Ti are considered conservative elements, i.e., rather immobile in weathering crust, the comparison of Ti/Al in sediments with Ti/Al in the UCC must respect segregation of those elements on weathering and transport (Rudnick and Gao, 2003). Titanium carriers are rather quickly released from parent rocks to finely particulate solid weathering products (Young and Nesbitt, 1998; Fralick and Kronberg, 1997), but Ti^{4+} solubility in soil profiles is lower than that of Al^{3+}, Fe^{n+}, and H_4SiO_4 and Ti thus do not readily form the finest nanoparticles. In fine sediments (silt-clay mixtures) of the Most Basin and the Amazon River, the Ti/Al ratio indeed gently decreases with increasing Al/Si (Fig. 5B). Consistent with that is the use of Ti/Al as grain-size proxy in distal marine sediments (Zabel et al., 2001; Xu et al., 2018), with Ti/Al elevated in coarser (silty) sediments compared to

clay. The Ti/Al ratios in sediments cannot be attributed exclusively to grain size because the Ti content in various rocks is quite variable, with considerably greater values in mafic rocks (Young and Nesbitt, 1998), mafic rocks are also Ti-rich in the Most Basin (Ulrych et al., 2002; Matys Grygar et al., 2016). Indeed, the values of Ti/Al in the Most Basin are elevated compared to those from the Amazon and Ganga-Brahmaputra rivers (Fig. 5B). Therefore, a certain part of Ti/Al variations in the Most Basin could also reflect some provenance control. Anyway, Ti/Al could only serve as a proxy for grain size if the sediment provenance is invariant.

The grain-size control on K concentrations depends substantially on the actual minerals carrying K. In mature sediments, the K concentration should be lower than that in the UCC and Al-normalised K concentrations should be gently decreasing with increasing Al/Si ratio due to K progressive leaching under maturation of clay minerals from illite via smectite to kaolinite. That gentle decrease is indeed observed in the Amazon River and the Most Basin sediments (Fig. 6). A clear provenance control is obvious from contrasting K/Al values in the Solimões and the Madeira rivers, the Amazon tributaries (Fig. 6B).

While normalisation of mobile element concentrations by Al is most common in weathering indices (Garzanti et al., 2013; Zhao et al., 2018), Ti normalisation was found to be better performing in the Most Basin chemostratigraphic correlations (Matys Grygar and Mach, 2013). Both Al and Ti will correct the element composition for varying concentrations of diluting components and suppress the texture effects in XRF. Titanium-normalised K concentrations in the Most Basin sediment increase with Al/Si as in the solids transported by the Amazon River, with that trend in the Most Basin being steeper (Fig. 7). The K/Al and K/Ti ratios in sedimentary record will show different sensitivity to provenance variations (Ti variations) and also different secondary “grain-size effect”, i.e., opposite change of K/Al and K/Ti in very fine sediments. As a consequence of the latter, K/Al is gently decreasing (Fig. 6B) and K/Ti is gently increasing with increasing Al/Si in the Amazon River sediments with

Al/Si > 0.3 (Fig. 7B). The performance of Al and Ti for normalisation of K should thus be tested empirically in any novel particular case study. Perhaps another normalising element(s) could be employed, because Ti may show provenance control and Al analysis may not feasible or reliable, such as in the use of XRF scanners, for which the determination of light elements including Al is a challenge (Hennekam and Lange, 2012).

4.2 Orbital signatures in individual element ratios in the Most Basin sediments

The lacustrine Most Basin deposits were accumulated for 1.8 My (Matys Grygar et al., 2017b, 2019), which was sufficiently long to expect they recorded orbital forcing in their chemical composition, in particular in chemical weathering proxies. Expression of individual orbital cycles in individual element proxies in one of the cores from the Most Basin, discussed in section 4.1, is shown in Fig. 8. The assignment of frequencies to orbital cycles includes knowledge of the mean deposition rate which is estimated as 18-19 cm/kyr in the upper part of HK591 drill core (Matys Grygar et al., 2014, 2017b). Individual element ratios show variability with a frequency compatible with those of obliquity (O, ca. 41 kyr), precession (P, ca. 20 kyr), and the first harmonics of precession called half-precession (HP) (Fig. 8). The signal of short eccentricity (e) is missing in the studied upper half of HK591, because in this period the eccentricity was persistently high and showed low variability in that particular time interval, as it is known from the astronomical solution by Laskar et al. (2004), and also because the analysed interval covered only 4 short eccentricity cycles.

In the analysed part of HK591, the grain-size proxies Al/Si and Zr/Rb mostly reflect the O periodicity (Fig. 8, major wavelength 8.22 m after division by mean sedimentation rate corresponds to 44 kyr), while P signal is weaker. The mixed provenance- and the grain-size proxy Ti/Al shows O and P signals of similar (weak) power as Al/Si. Chemical weathering proxies K, K/Al, and K/Ti show mainly P signal and less O signal, all with powers considerably exceeding those of the grain size proxies. The K normalisation by Ti shows better

performance in suppressing “noise” in the power spectra (Fig. 8). Varying weights of orbital cycles in individual element ratios can be attributed to different physical mechanisms by which the orbital cycles affect individual components of the sediment production, delivery, and deposition in the Most Basin floor.

Distinct expression of orbital signals in grain-size and weathering proxies documents their partial independence and larger power of the raw and normalised K concentrations compared to the Al/Si, Zr/Rb, and Ti/Al ratios in the Most Basin demonstrates the K variations are not primarily controlled by grain size nor provenance. Contrarily to those findings, very similar element patterns and spectrograms were found by Zabel et al. (2001) for K/Al, Ti/Al, and Zr/Al and Colin et al. (2014) for Si/Al, K/Al, Ti/Al, and clay mineral ratios in African offshore marine sediments, probably because all those factors were mostly controlled by their variable grain size. The major grain-size control does not allow simple interpretation of weathering intensity in terms of humidity.

4.3 Checklist for interpretation of K concentrations in sediments

The preceding sections (4.1 and 4.2) can be converted to checklist or a sequence of steps that should be applied if K concentrations in siliciclastic sediments are considered as a possible paleoclimate record.

Step 1: a grain-size proxy must be established, because it can control the sediment composition (Bouchez et al., 2011; Tanaka and Watanabe, 2015; Matys Grygar and Popelka, 2016). A grain size proxy is essential for most subsequent steps in this checklist. To use conventional Al/Si, the possible presence of biogenic or chemogenic silica must be excluded. The presence of biogenic structures may be examined by microscopy (Xu et al., 2018). Biogenic silica would cause specific departures to the left from the hyperbolic trajectory in Zr/Rb vs. Al/Si plots (Fig. 3) and to the top from the quartz-kaolinite line in Fig.

4B. If biogenic silica is present, Zr/Rb or sometimes Ti/Al (Xu et al., 2018) may substitute for Al/Si in silt-clay mixtures.

Step 2: the grain-size control on Ti/Al should be examined, as it may help to reveal a geological provenance control. In mature sediments, a single trajectory of Ti/Al against the grain-size proxy, typically a flat dependence with a final gentle decrease in the finest sediments, could indicate the grain-size control on the Ti concentration (Zabel et al., 2001; Xu et al., 2018). Scatter or other distinct patterns in Ti concentrations or concentration ratios could indicate provenance variability (Young and Nesbitt, 1998; Matys Grygar et al., 2016) or very low sediment maturity, which both would make any weathering proxy equivocal. This work does not include a review of a broad suite of other provenance tracers, but whatever of them may meet the requirements of this step.

Step 3: the grain-size control on K must be examined. A single trajectory of K/Al gently decreasing with sediment fining (data in Bouchez et al., 2011; Garzanti et al., 2013; Guo et al., 2018) could indicate prevalent grain-size control over sediment composition, such as in data by Zabel et al. (2001) and Colin et al. (2014). Exclusive grain-size control of chemical composition could also reflect climate changes, but would devaluate weathering indices. Vice versa, scattered K/Al independent on grain size and stronger power of orbital signals in K concentrations than in the grain-size proxies, as what is actually obtained in the Most Basin (Fig. 6), can confirm the desired climatic content of K-based weathering index.

Step 4: the relationship between K and Rb should be examined, e.g., as scatter plots of K/Rb vs. a grain-size proxy (Fig. 9A). If the K/Rb ratio is not stable and tends to be larger than that in the UCC, post-sedimentary enrichment by K (metasomatism) could have acted (van den Kamp, 2016). The impact of metasomatism was also evaluated using A-CN-K plots (Fedo et al., 1995, also used by Zhao et al., 2018), microscopic examination of clay mineral particles to distinguish their detrital and autochthonous origin (Martínez-Braceras et al., 2017; Wang et al., 2017), and mineral (micro)analysis (Kříbek et al., 2017; Foerster et al., 2018) to

identify possible neo-formed K-rich phases. The K/Rb 100-200, i.e., lower than in the UCC, and its gentle decrease with the sediment fining from silt to clay (cf. Fig. 9B), can be due to preferential leaching of K over Rb during weathering (Gaillardet et al., 1999; Garzanti et al., 2013; Clift et al., 2014; Tanaka and Watanabe, 2015). In evaluation of K/Rb ratio in sediments, sediment provenance must also be considered, as, e.g., granitic rocks are specific (Tanaka and Watanabe, 2015).

Step 5: suitable normalisation element for depth profiles of K concentration should be selected to correct for varying dilution effects and grain-size control, such as Al and Ti with only minor (and opposite) secondary grain-size control by Al/Si (cf. Fig. 6B and Fig. 7B). The normalisation element must be insoluble during weathering and transport from the sediment source area and show similar grain size preference as K, that is not the case of elements carried mainly by heavy minerals. Performance of the normalisation element must be verified empirically, e.g., as shown in subsequent steps of this list. Both Al and Ti concentrations may reflect sediment provenance. In the case study by Zhao et al. (2018), K/Al was not particularly sensitive to provenance change, while opposite was valid in the above discussed example of the Amazon River tributaries. There no need to always eliminate the provenance control from compositional data analysis, because switching between sediment source areas (geographical provenances) may actually represent one of possible climate-recording mechanisms (Colin et al., 2014; Zhao et al., 2018), but then K concentrations lost their weathering intensity content.

Step 6: the “lateral stability” (spatial invariance) of the normalised K concentrations in sediments should be tested. Well-performing paleoclimate proxy must show lateral stability from basin centre to periphery or among individual depocentres as in the Most Basin (Matys Grygar and Mach, 2013; Matys Grygar et al., 2017a, 2017b). Insight into the basin architecture is here equally important as in distinguishing eustatic sea-level patterns from other controlling factors in near-shore marine basins (Uličný et al., 2009). Autogenic cycles

in basin filling or local tectonics (Alonso-Zarza et al., 2012; Valero et al., 2017) would result in lateral instability of weathering signals and their devaluation.

Step 7: independent test of climatic controls. Spectral analysis should be performed in chemical depth profiles in siliciclastic sediments, if these records cover sufficiently long time interval (Fig. 8). The climate content of weathering indices can be verified by their comparison with global climatic curves (Clift et al., 2014; Matys Grygar et al., 2017b, 2019), which can also be applied to sediment series covering shorter time intervals, such as recent centuries to millennia (Bábek et al., 2011; Zhao et al., 2018)

4.4 Limits of weathering indices

The composition of continental and continent-derived sediments reflects the interplay between geology, paleotopography, and precipitation patterns, which in turn controls the sediment source area and sediment transport paths in a site-specific interplay (Colin et al., 2014; Zhao et al., 2018). Those factors are not known for the more remote past. The most relevant mechanisms acting here are slow rate of chemical weathering, sediment recycling, and sorting of sediment components on transport. While Pleistocene interglacials and interstadials (millennial timescale) are clearly discernible in soil and sediment geochemistry and mineralogy even in the cold to temperate climate (Bábek et al., 2011; Hošek et al., 2015), the Younger Dryas (centennial timescale) may not be recorded (Zhao et al., 2018). If short climatic events are present in sediment geochemistry and mineralogy, they likely result from changed provenance and transport paths rather than climate itself. The acquisition of climate signal is also affected by source area topography. Steep terrains can produce less mature sediments than expected (Garzanti and Resentini, 2016; von Eynatten et al., 2016). Vice versa, repeated recycling and weathering in flat areas enhance sediment maturation (Gaillardet et al., 1999; Zhao et al., 2018). The transport of sediments may result in hydrodynamic sorting of sediment components, such as larger particles of kaolinite and illite and smaller particles of smectite and illite/smectite (Martínez-Braceras et al.,

2017; Wang et al., 2017). The finest particles may be selectively removed from deposits subjected even to slow currents after deposition. The sorting effects could be revealed by grain size control over the entire chemical composition of sediments and by their lateral chemical heterogeneity in the studied basin.

Other mobile elements than K may also be suitable for weathering indices. Gaillardet et al. (1999) showed that potassium is not much depleted in weathering products formed in areas with mean annual temperature lower than ca. 10 °C. For cold or arid climates, Na concentration in fine sand or silt fractions could then be tested. Indeed, Na and non-carbonate Ca reflected climate drying from the Miocene via Pliocene to Pleistocene in the loess/soils in the China Loess Plateau, while K concentration was nearly constant there (Liang et al., 2009). In tropical climate of Angola, equatorial coast of Africa, Mg concentration in fluvial muds show correlation with average annual precipitation, as follows from data published by Dinis et al. (2017). The same principles as in the checklist for K should, however be valid for any other mobile element. The topic of weathering indices in sedimentary records is thus definitely not exhausted.

5. Conclusion

The element geochemistry of siliciclastic continental sediments mostly composed of clay- and silt-sized particles results from an interplay between several controlling factors, of which the complete deciphering for ancient depositional environments may not be possible. One of the factors controlling the K concentration in mature sediments is, however, chemical weathering intensity in the sediment source area. We showed how to evaluate the grain-size and provenance controls of K concentrations and their possible post-depositional alteration, all being attainable by geochemical normalisation. After performing those steps, the K concentration may provide a signal related to chemical weathering intensity, which has a potential to record the paleoclimate. If the interplay of

factors behind K concentrations cannot be deciphered, the climatic content in K concentrations cannot be extracted. Even in such case, K-stratigraphy can provide an intrabasin chemostratigraphic correlation and allow for identification of orbital pacing in sufficiently long records, which can be optimised by proper geochemical normalisation. For sediments produced other climates than dealt with in our work, under which K was insufficiently mobile or too mobile, attention could be focused on other ions such as Na or Mg, but the same factors as those controlling the K concentrations should be considered.

Acknowledgment

The work was supported by Czech Science Foundation (project number 16-00800S). VODAMIN project and North Bohemian Mines generously provided drill cores from the Most Basin and gave the authors permission to use them for scientific purposes for free. The authors thank to M. Faměra, M. Hošek, M. Maříková, and P. Vorm from the workplace of corresponding author to perform sampling of drill cores, sample laboratory processing, and XRF analysis. The authors thank to an anonymous reviewer for constructive comments.

References

Abels, H. A., Hilgen, F. J., Krijgsman, W., Kruk, R. W., Raffi, I., Turco, E., Zachariasse, W. J., 2005. Long-period orbital control on middle Miocene global cooling: Integrated stratigraphy and astronomical tuning of the Blue Clay Formation on Malta, Paleoceanogr. 20, PA4012. doi:10.1029/2004PA001129.

Abels, H. A., Abdul Aziz, H., Krijgsman, W., Smeets, S. J. B., Hilgen, F., 2010. Long-period eccentricity control on sedimentary sequences in the continental Madrid Basin (middle Miocene, Spain). Earth Planet. Sci. Lett. 289, 220–231.

Abels, H. A., Kraus, M. J., Gingerich, P. D., 2013. Precession-scale cyclicity in the fluvial lower Eocene Willwood Formation of the Bighorn Basin, Wyoming (USA). Sedimentology 60, 1467–1483.

Alonso-Zarza, A. M., Meléndez, A., Martín-García, R., Herrero, M. J., and Martín-Pérez, A., 2012. Discriminating between tectonism and climate signatures in palustrine deposits: lessons from the Miocene of the Teruel Graben, NE Spain. Earth Sci. Rev. 113, 141–160.

Bábek, O., Chlachula, J., Grygar, T. M., 2011. Non-magnetic indicators of pedogenesis related to loess magnetic enhancement and depletion: Examples from the Czech Republic and southern Siberia Quatern. Sci. Rev. 30, 967–979.

Baumgarten, H., Wonik, T., Tanner, D. C., Francke, A., Wagner, B., Zanchetta, G., Sulpizio, R., Giaccio, B., Nomade, S., 2015. Age–depth model of the past 630 kyr for Lake Ohrid (FYROM/Albania) based on cyclostratigraphic analysis of downhole gamma ray data. Biogeosci. 12, 7453–7465.

Bouchez, J., Gaillardet, J., France-Lanord, C., Maurice, L., Dutra-Maia, P., 2011. Grain size control of river suspended sediment geochemistry: Clues from Amazon River depth profiles. Geochem. Geophys. Geosyst. 12, Q03008, doi:10.1029/2010GC003380.

Chen, J., Chen, Y., Liu, L.-W., Ji, J.-F., Balsam, W., Sun, Y.-B., Lu, H.-Y., 2006. Zr/Rb ratio in the Chinese loess sequences and its implication for changes in the East Asian winter monsoon strength. Geochim. Cosmochim. Acta 70, 1471-1482.

Clift, P. D., Wan, S.-M., Blusztajn, J., 2014. Reconstructing chemical weathering, physical erosion and monsoon Earth Sci. Rev. 130, 86–102.

Colin, C., Siani, G., Liu, Z.-F., Blamart, D., Skonieczny, C., Zhao, Y.-L., Bory, A., Frank, N., Duchamp-Alphonse, S., Thil, F., Richter, T., Kissel, C., Gargani, J., 2014. Late Miocene to early Pliocene climate variability off NW Africa (ODP Site 659). Palaeogeogr. Palaeoclimatol. Palaeoecol. 401, 81–95.

Cuadros, J., Andrade, G., Ferreira, T. O., de Moya Partiti, C. S., Cohen, R., Vidal-Torrado, P., 2017. The mangrove reactor: Fast clay transformation and potassium sink. Appl. Clay Sci. 140, 50–58.

De Vleeschouwer, D., Vahlenkamp, M., Crucifix, M., Pälike, H., 2017. Alternating Southern and Northern Hemisphere climate response to astronomical forcing during the past 35 m.y. Geology 45, 375–378.

Dèzes, P., Schmid, S.M., Ziegler, P.A., 2004. Evolution of the European Cenozoic Rift System: interaction of the Alpine and Pyrenean orogens with their foreland lithosphere. Tectonophys. 389, 1–33.

Dinis, P., Garzanti, E., Vermeesc, P., Huvi, J., 2017. Climatic zonation and weathering control on sediment composition (Angola). Chemical Geology 467, 110-121.

Fedo, C. M., Nesbitt, H. W., Young, G. M., 1995. Unravelling the effects of potassium metasomatism in sedimentary rocks and paleosols, with implications for paleoweathering conditions and provenance. Geology 23, 921–924.

Fralick, P., Kronberg, B., 1997. Geochemical discrimination of clastic sedimentary rock sources. Sediment. Geol. 113, 111–124.

Foerster, V., Vogelsang, R., Junginger, A., Asrat, A., Lamb, H. F., Schaebitz, F., Trauth, M. H., 2015. Environmental change and human occupation of southern Ethiopia and northern Kenya during the last 20,000 years. Quatern. Sci. Rev. 129, 333–340.

Foerster, V., Deocampo, M., Asrat, A., Günter, C., Junginger, A., Krämer, K. H., Stroncik, N. A., Trauth, M. H., 2018. Towards an understanding of climate proxy formation in the Chew Bahir basin, southern Ethiopian Rift. Palaeogeogr. Palaeoclimatol. Palaeoecol. 501, 111–123.

Gaillardet, J., Dupré, B., Allègre, C. J., 1999. Geochemistry of large river suspended sediments: silicate weathering or recycling tracer? Geochimica et Cosmochimica Acta 63, 4037-4051.

Gärtner, A., Linnemann, U., Sagawe, A., Hofmann, M., Ullrich, B., Kleber, A., 2013. Morphology of zircon crystal grains in sediments – characteristics, classifications, definitions. Geol. Saxonica 59, 65-73.

Garzanti, E., Resentini, A., 2016. Provenance control on chemical indices of weathering (Taiwan river sands). Sedim. Geol. 336, 81–95.

Garzanti, E., Andó, S., France-Lanord, C., Censi, P., Vignola, P., Galy, V., Lupker, B., 2011. Mineralogical and chemical variability of fluvial sediments 2. Suspended-load silt (Ganga–Brahmaputra, Bangladesh). Earth Planet. Sci. Lett. 302, 107–120.

Garzanti, E., Padoan, M., Peruta, L., Setti, M., Najman, Y., Villa, I. M., 2013. Weathering geochemistry and Sr-Nd fingerprints of equatorial upper Nile and Congo muds. Geochem. Geophys. Geosyst. 14, 292–316.

Guo, Y.-L., Yang, S.-Y., Su, N., Li, C., Yin, P., Wang, Z.-B., 2018. Revisiting the effects of hydrodynamic sorting and sedimentary recycling on chemical weathering indices. Geochim. Cosmochim. Acta 227, 48–63.

Hennekam, R., de Lange, G., 2012. X-ray fluorescence core scanning of wet marine sediments: methods to improve quality and reproducibility of high resolution paleoenvironmental records. Limnol. Oceanogr. Methods 10, 991–1003.

Hošek, J., Hambach, U., Lisá, L., Grygar, T. M., Horáček, I., Meszner, S., Knésl, I., 2015. An integrated rock-magnetic and geochemical approach to loess/paleosol sequences from Bohemia and Moravia (Czech Republic): Implications for the Upper Pleistocene paleoenvironment in central Europe. Palaeogeogr. Palaeoclimatol. Palaeoecol. 418, 344–358.

Kříbek, B., Knésl, I., Rojík, P., Sýkorová, I., Martínek, K., 2017. Geochemical history of a Lower Miocene lake, the Cypris Formation, Sokolov Basin, Czech Republic. J. Paleolimnol. 58, 169–190.

Kwiecien, O., Stockhecke, M., Pickarski, N., Heumann, G., Litt, T., Sturm, M., Anselmetti, F., Kipfer, R., Haug, H. G., 2015. Dynamics of the last four glacial terminations recorded in Lake Van, Turkey. Quatern. Sci. Rev. 104, 42–52.

Larsen, D., 2008, Revisiting silicate authigenesis in the Pliocene–Pleistocene Lake Tecopa beds, southeastern California: Depositional and hydrological controls. Geosphere 4, 612–639.

Laskar, J., Robutel, P., Joutel, F., Gastineau, M., Correia, A. C. M., Levrard, B., 2004. A long-term numerical solution for the insolation quantities of the Earth. Astronomy Astrophys. 428, 261–285.

Liang, M., Guo, Z., Kahmann, A. J., Oldfield, F, 2009. Geochemical characteristics of the Miocene eolian deposits in China: Their provenance and climate implications. Geochem. Geophys. Geosyst. 10, Q04004, doi:10.1029/2008GC002331.

Miller, K. G., Baluyot, R., Wright, J. D., Kopp, R. E., Browning, J. V., 2017. Closing an early Miocene astronomical gap with Southern Ocean $\delta^{18}O$ and $\delta^{13}C$ records: Implications for sea level change. Paleoceanogr. 32, 600–621.

Mach, K., Teodoridis, V., Matys Grygar, T., Kvaček, Z., Suhr, P., Standke, G. 2014. An evaluation of paleogeography and paleoecology in the Most Basin (Czech Republic) and Saxony (Germany) from the late Oligocene to the early Miocene. Ne. Jb. Geol. Paläontol. Abh. 272, 13–45.

Martínez-Braceras, N., Payros, A., Miniati, F., Arostegi, J., Franceschetti, G., 2017. Contrasting environmental effects of astronomically driven climate change on three Eocene hemipelagic successions from the Basque–Cantabrian Basin. Sedimentology 64, 960–986.

Matys Grygar, T., Mach, K., 2013. Regional chemostratigraphic key horizons in the macrofossil-barren siliciclastic lower Miocene lacustrine sediments (Most Basin, Eger Graben, Czech Republic). Bull. Geosci. 88, 557–571.

Matys Grygar, T., Popelka, J., 2016, Revisiting geochemical methods of distinguishing natural concentrations and pollution by risk elements in fluvial sediments. J. Geochem. Explor. 170, 39–57.

Matys Grygar, T., Mach, K., Pruner, P., Schnabl, P., Laurin, J., Martinez, M. 2014. A lacustrine record of the early stage of the Miocene Climatic Optimum in Central Europe from the Most Basin, Ohře (Eger) Graben, Czech Republic. Geol. Mag. 151, 1013–1033.

Matys Grygar, T., Elznicová, J., Kiss, T., Smith, H.G., 2016. Using sedimentary archives to reconstruct pollution history and sediment provenance: The Ohře River, Czech Republic. Catena 144, 109–129.

Matys Grygar, T., Mach, K., Hošek, M., Schnabl, P., Martinez, M., Koubová, M., 2017a. Early stages of clastic deposition in the Most Basin (Ohře Rift, Czech Republic, Early Miocene): timing and possible controls. Bull. Geosci. 92, 337–355.

Matys Grygar, T., Hošek, M. Mach, K., Schnabl, P., Martinez, M., 2017b. Climatic instability before the Miocene Climatic Optimum reflected in a Central European lacustrine record from the Most Basin in the Czech Republic. Palaeogeogr. Palaeoclimatol. Palaeoecol. 485, 930–945.

Matys Grygar, T., Hošek, M., Pacina, J., Štojdl, J., Bábek, O., Sedláček, J., Hron, K., Talská, R., Kříženecká, S., Tolaszová, J., 2018. Changes in the geochemistry of fluvial sediments after dam construction (the Chrudimka River, the Czech Republic). Appl. Geochem. 98, 94-108.

Matys Grygar, T., Mach, K., Schnabl, P., Martinez, M., Zeeden, C., 2019. Orbital forcing and abrupt events in a continental weathering proxy from central Europe (Most Basin, Czech Republic, 17.7–15.9 Ma) recorded beginning of the Miocene Climatic Optimum. Palaeogeogr. Palaeoclimatol. Palaeoecol. 514, 423–440.

Meyers, S.R., 2012. Seeing red in cyclic stratigraphy: spectral noise estimation for astrochronology. Paleoceanogr. 27, PA3228.

Rajchl, M., Uličný, D., Grygar, R., Mach, K., 2009. Evolution of basin architecture in an incipient continental rift: the Cenozoic Most Basin, Eger Graben (Central Europe). Basin Res. 21, 269–294.

Rudnick, R., Gao, S., 2003. Composition of the continental crust. In: Rudnick, R.L., Holland, H.D., Turekian, K.K. (Eds.), The Crust. Treatise on Geochemistry 3. Elsevier–Pergamon, Oxford, pp. 1–64.

Stockhecke, M., Kwiecien, O., Vigliotti, L., Anselmetti, F. S., Beer, J., Namik Çağatay, M., Channell, J. E. T., Kipfer, R., Lachner, J., Litt, T., Pickarski, N., Sturm, M., 2014. Chronostratigraphy of the 600,000 year old continental record of Lake Van (Turkey). Quatern. Sci. Rev. 104, 8–17.

Sun, Y., Ma L., Bloemendal, J., Clemens, S., Qiang, X., An, Z., 2015. Miocene climate change on the Chinese Loess Plateau: Possible links to the growth of the northern Tibetan Plateau and global cooling. Geochem. Geophys. Geosyst. 16, 2097–2108.

Tanaka, K., Watanabe, N., 2015. Size distribution of alkali elements in riverbed sediment and its relevance to fractionation of alkali elements during chemical weathering. Chem. Geol. 411, 12-18.

Taner, M. T., 2003. Attributes Revisited, Technical Publication. Houston, Texas: Rock Solid Images, Inc. Available at:http://rocksolidimages.com/pdf/attrib_revisited.htm.

Teodoridis, V., Kvaček, Z., 2015. Palaeoenvironmental evaluation of Cainozoic plant assemblages from the Bohemian Massif (Czech Republic) and adjacent Germany. Bull. Geosci. 90, 695–720.

Thomson, D. J., 1982. Spectrum estimation and harmonic analysis. Proc. IEEE 70, 1055–1096.

Thomson, D. J., 1990. Quadratic-inverse spectrum estimates – applications to paleoclimatology. Phil. Trans. Royal Soc. A Math. Phys. Eng. Sci. 332, 539–597.

Uličný, D., Laurin, J., Čech, S., 2009. Controls on clastic sequence geometries in a shallow-marine, transtensional basin: The Bohemian Cretaceous Basin, Czech Republic. Sedimentology 56, 1077–1114.

Ulrych, J., Svobodová, J., Balogh, K., 2002. The source of Cenozoic volcanism in the České středohoří Mts., Bohemian Massif. N. Jb. Miner. Abh. 177, 133–162.

Ulrych, J., Dostal, J., Adamovič, J., Jelínek, E., Špaček, P., Hegner, E., Balogh, K., 2011. Recurrent Cenozoic volcanic activity in the Bohemian Massif (Czech Republic). Lithos 123, 133–144.

Valero, L., Garcés, M., Cabrera, L., Costa, E., Sáez, A., 2014. 20 Myr of eccentricity paced lacustrine cycles in the Cenozoic Ebro Basin. Earth Planet. Sci. Lett. 408, 183–193.

Valero, L., Huerta, P., Garcés, M., Armenteros, I., Beamud, E., Gómez-Paccard, M. 2017. Linking sedimentation rates and large-scale architecture for facies prediction in nonmarine basins (Paleogene, Almazán Basin, Spain). Basin Res. 29, 213–232.

van den Kamp, P. C., 2016. Potassium distribution and metasomatism in pelites and schists: how and when, relation to postdepositional events. J. Sedim. Res. 86, 683–711.

Vögeli, N., van der Beek, P., Huyghe, P., Najman, Y., 2017. Weathering in the Himalaya, an East-West Comparison: Indications from Major Elements and Clay Mineralogy. J. Geol. 125, 515–529.

von Eynatten, H., Tolosana-Delgado, R., Karius, V., Bachmann, K., Caracciolo L, 2016. Sediment generation in humid Mediterranean setting: Grain-size and source-rock control on sediment geochemistry and mineralogy (Sila Massif, Calabria). Sedim. Geol. 336, 68–80

Wang, C.-W., Adriaens, R., Hong, H.-L., Elsen, J., Vandenberghe, N., Lourens, L. J., Gingerich, P. D., Abels, H. A., 2017. Clay mineralogical constraints on weathering in response to early Eocene hyperthermal events in the Bighorn Basin, Wyoming (Western Interior, USA). GSA Bull. 129, 997–1011.

Wilhelms-Dick, D., Westerhold, T., Röhl, U., Wilhelms, F., Vogt, C., Hanebuth, T. J. J., Römmermann, H., Kriewsm M., Kasten, S., 2012. A comparison of mm scale resolution techniques for element analysis in sediment cores. J. Anal. At. Spectrom. 27, 1574-1584.

Xu, W., Ruchl, M., Jenkyns, H. C., Leng, M. J., Huggett, J. M., Minisini, D., Ullmann, C. V., Diding, J. B., Weijers, J. W. H., Storm, M. S., Percival, L. M. E., Tosca, N. J., Idiz, E. F., Tegelaar, E. W., Hasselbo, S. P., 2018. Evolution of the Toarcian (Early Jurassic) carbon-cycle and global climatic controls on local sedimentary processes (Cardigan Bay Basin, UK). Earth Planet. Sci. Lett. 484, 396–411.

Young, G. M., Nesbitt, H. W., 1998. Processes controlling the distribution of Ti and Al in weathering profiles, siliciclastic sediments and sedimentary rocks. J. Sedim. Res. 68, 448–455.

Zabel, M., Schneider, R. R., Wagner, T., Adegbie, A. T., de Vries, U., Kolonic, S., 2001. Late Quaternary Climate Changes in Central Africa as Inferred from Terrigenous Input to the Niger Fan. Quaternary Res. 56, 207–217.

Zachos, J., Pagani, M., Sloan, L., Thomas, E., Billups, K., 2001. Trends, rhythms, and aberrations in global climate 65 Ma to present. Science 292, 686–693.

Zhao, D., Wan, S., Clift, P. D., Tada, R., Huang, J., Yin, X., Liao, R., Shen, X., Shi, X., Li, A., 2018. Provenance, sea-level and monsoon climate controls on silicate weathering of Yellow River sediment in the northern Okinawa Trough during late last glaciation. Palaeogeogr. Palaeoclimatol. Palaeoecol. 490, 227–239.

Fig. 1. Map of the Most Basin with position of studied cores.

Fig. 2. Lithology and chemostratigraphic markers in the siliciclastic sediments above the Main Coal Seam if the Most Basin (A), their environmental assignment (B) and local stratigraphic scheme (C).

Fig. 3. Indirect proportionality of grain-size proxies in the Most Basin (A) and their comparison with reference data (B). Note logarithmic scale in y axis.

Fig. 4. Plot of Al vs. Si in the Most Basin raw data (A) and data after subtraction of siderite percentage calculated from Fe content (B). The main drivers of Al vs. Si are grain size and composition of clay mineral assemblage.

Fig. 5. Plot of Ti/Al vs. Al/Si in the Most Basin (A) and their comparison with reference data (B). All datasets show Ti/Al enrichment with respect to UCC (Rudnick and Gao, 2003) for Al/Si <0.3 and Ti/Al decline at Al/Si >0.3, particularly pronounced in the Most Basin sediments.

Fig. 6. Plot of K/Al vs. Al/Si in the Most Basin (A) and their comparison with reference data (B). K/Al plot vs. Al/Si shows scatter for the Most Basin sediments and lack of grain size control (A). The Most Basin sediments and finer Amazon River sediments show K depletion in finer fractions compared to UCC according to Rudnick and Gao (2003) (B).

Fig. 7. Plot of K/Ti vs. Al/Si in the Most Basin (A) and their comparison with reference data (B). The Most Basin sediments have elevated Ti concentration and correspondingly decreased K/Ti relative to reference sediments.

Fig. 8. Prewhitened 2π-MTM spectra of various geochemical proxies measured in core HK591 core part above C2 bed (its position is shown in Fig. 2) with confidence levels calculated using the LOWSPEC method (Meyers, 2012). Normalisation of K by Al and Ti improves separation of orbital frequencies from noise. Individual element ratios

show specific orbital signatures. The numbers near peaks show wavelength of the identified orbital cycles in metres.

Fig. 9. Plot of K/Rb vs. Al/Si in the Most Basin (A) and their consistence with the reference data (B). Note logarithmic scale in y axis. Gentle decline of K/Rb with growing fineness and kaolinite content is consistent with lower solubility of Rb under chemical weathering. The samples with elevated K/Rb in the Most Basin are those with siderite enrichment.

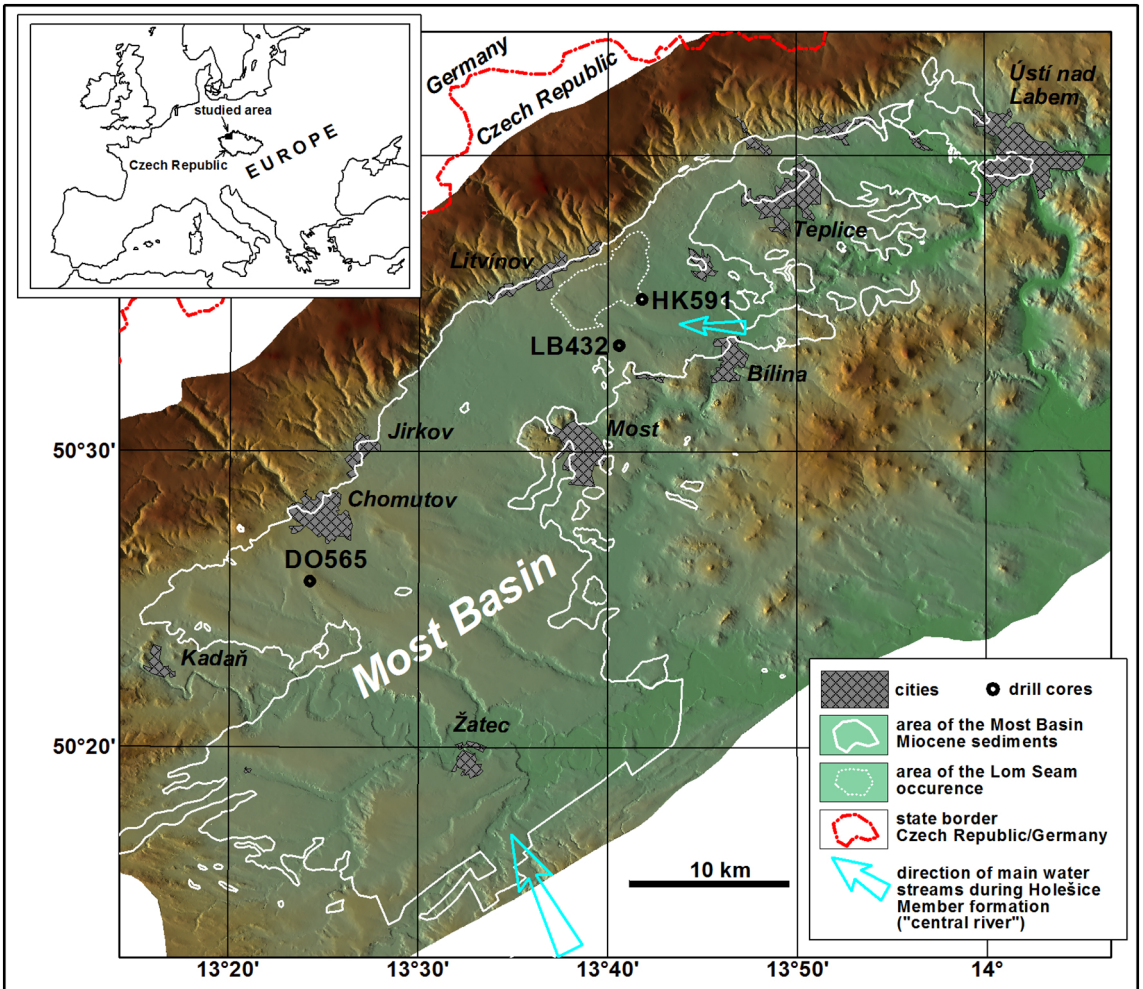
studied area
Czech Republic
EUROPE
Germany
Czech Republic
Ústí nad Labem
Teplice
Litvínov
HK591
LB432
Bílina
Jirkov
Most
Chomutov
DO565
Most Basin
Kadaň
Žatec
50°30'
50°20'
13°20'
13°30'
13°40'
13°50'
14°
10 km
cities
drill cores
area of the Most Basin Miocene sediments
area of the Lom Seam occurence
state border Czech Republic/Germany
direction of main water streams during Holešice Member formation ("central river")

Figure 1

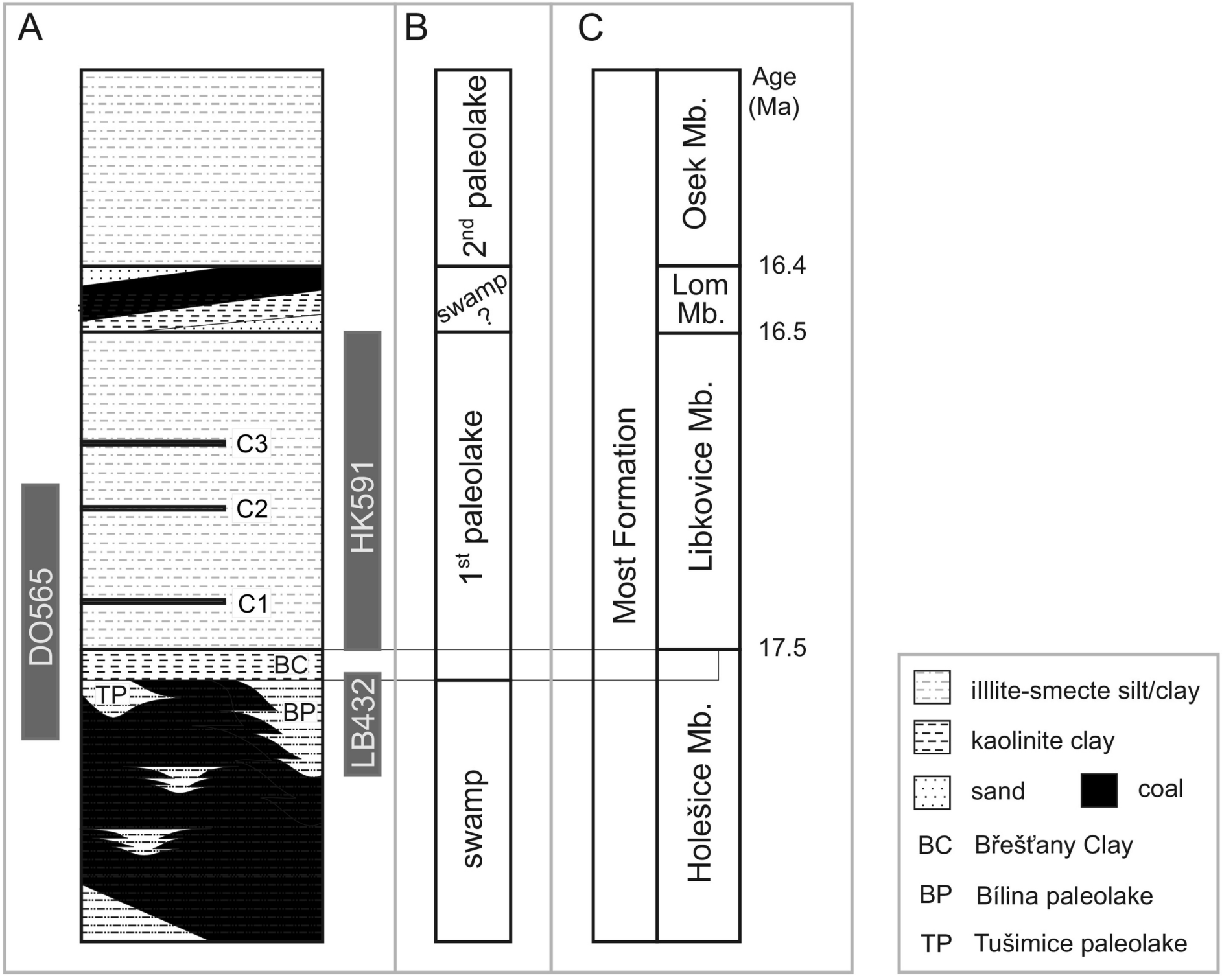
A
B
C
DO565
HK591
LB432
C3
C2
C1
BC
TP
BP
2nd paleolake
swamp
1st paleolake
swamp
Most Formation
Osek Mb.
Lom Mb.
Libkovice Mb.
Holešice Mb.
Age (Ma)
16.4
16.5
17.5
illlite-smecte silt/clay
kaolinite clay
sand
coal
BC Břešťany Clay
BP Bílina paleolake
TP Tušimice paleolake

Figure 2

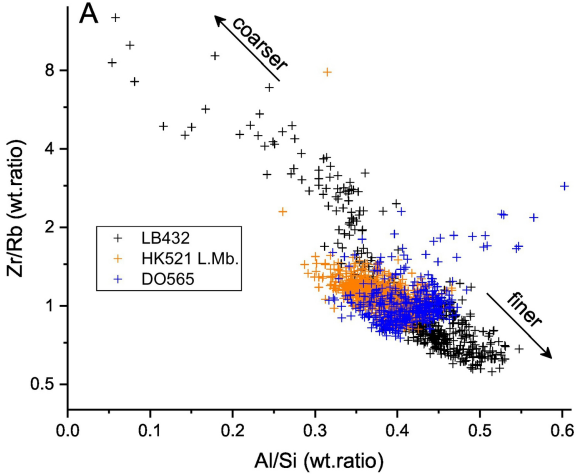

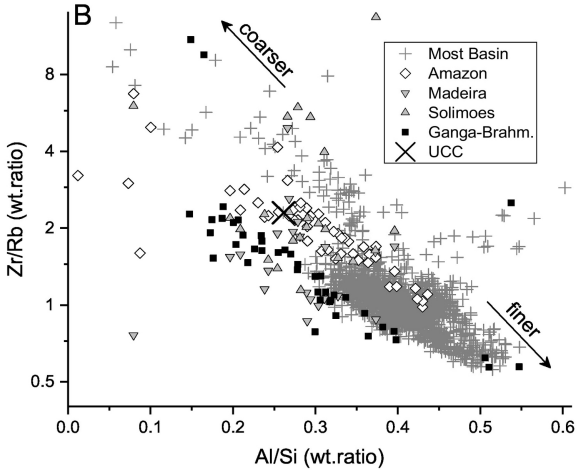

SED05442

Figure 3

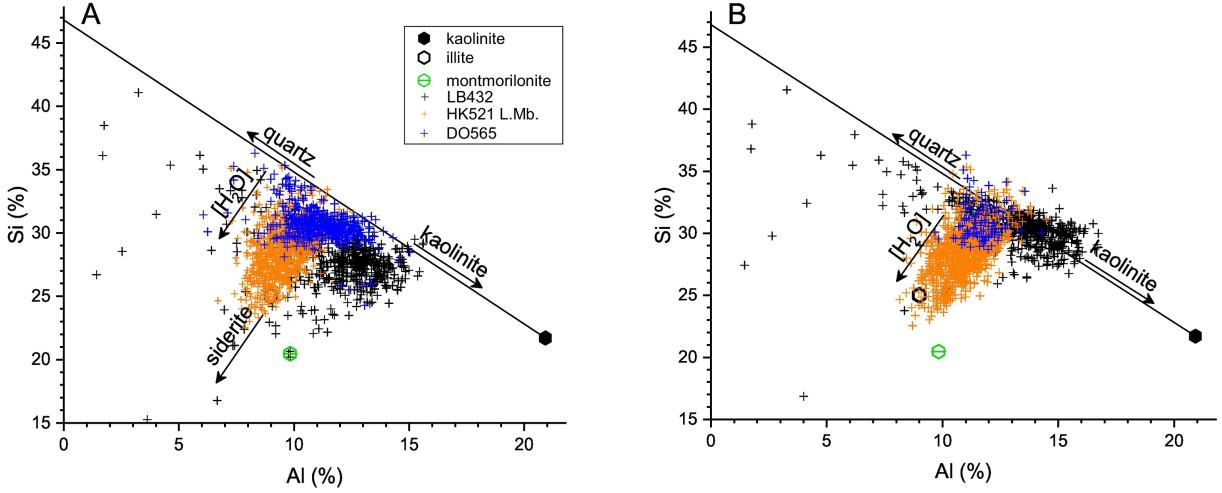
A
B
kaolinite
illite
montmorilonite
LB432
HK521 L.Mb.
DO565
quartz
kaolinite
siderite
[H2O]
Si (%)
Al (%)
0
5
10
15
20
15
20
25
30
35
40
45

Figure 4

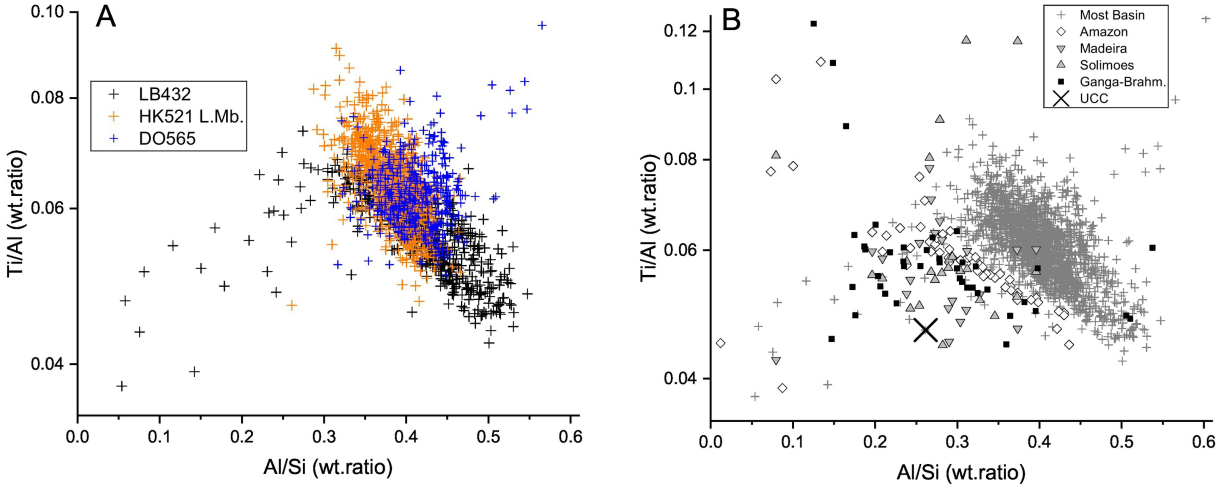
A
LB432
HK521 L.Mb.
DO565
Ti/Al (wt.ratio)
Al/Si (wt.ratio)
0.10
0.08
0.06
0.04
0.0
0.1
0.2
0.3
0.4
0.5
0.6
B
Most Basin
Amazon
Madeira
Solimoes
Ganga-Brahm.
UCC
Ti/Al (wt.ratio)
Al/Si (wt.ratio)
0.12
0.1
0.08
0.06
0.04

Figure 5

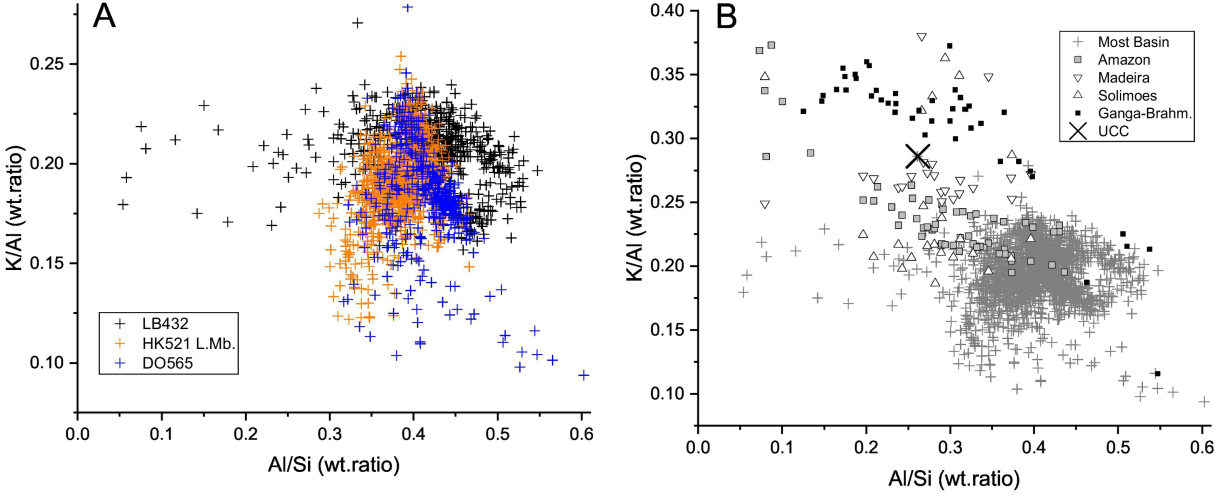
A
K/Al (wt.ratio)
Al/Si (wt.ratio)
LB432
HK521 L.Mb.
DO565
B
K/Al (wt.ratio)
Al/Si (wt.ratio)
Most Basin
Amazon
Madeira
Solimoes
Ganga-Brahm.
UCC

Figure 6

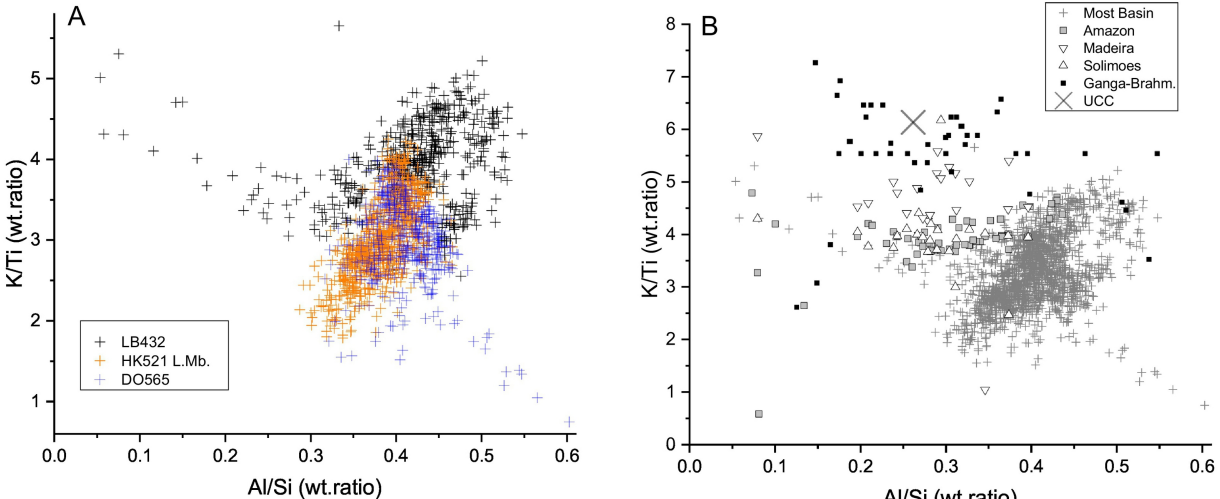
A
K/Ti (wt.ratio)
Al/Si (wt.ratio)
LB432
HK521 L.Mb.
DO565
B
K/Ti (wt.ratio)
Al/Si (wt.ratio)
Most Basin
Amazon
Madeira
Solimoes
Ganga-Brahm.
UCC

Figure 7

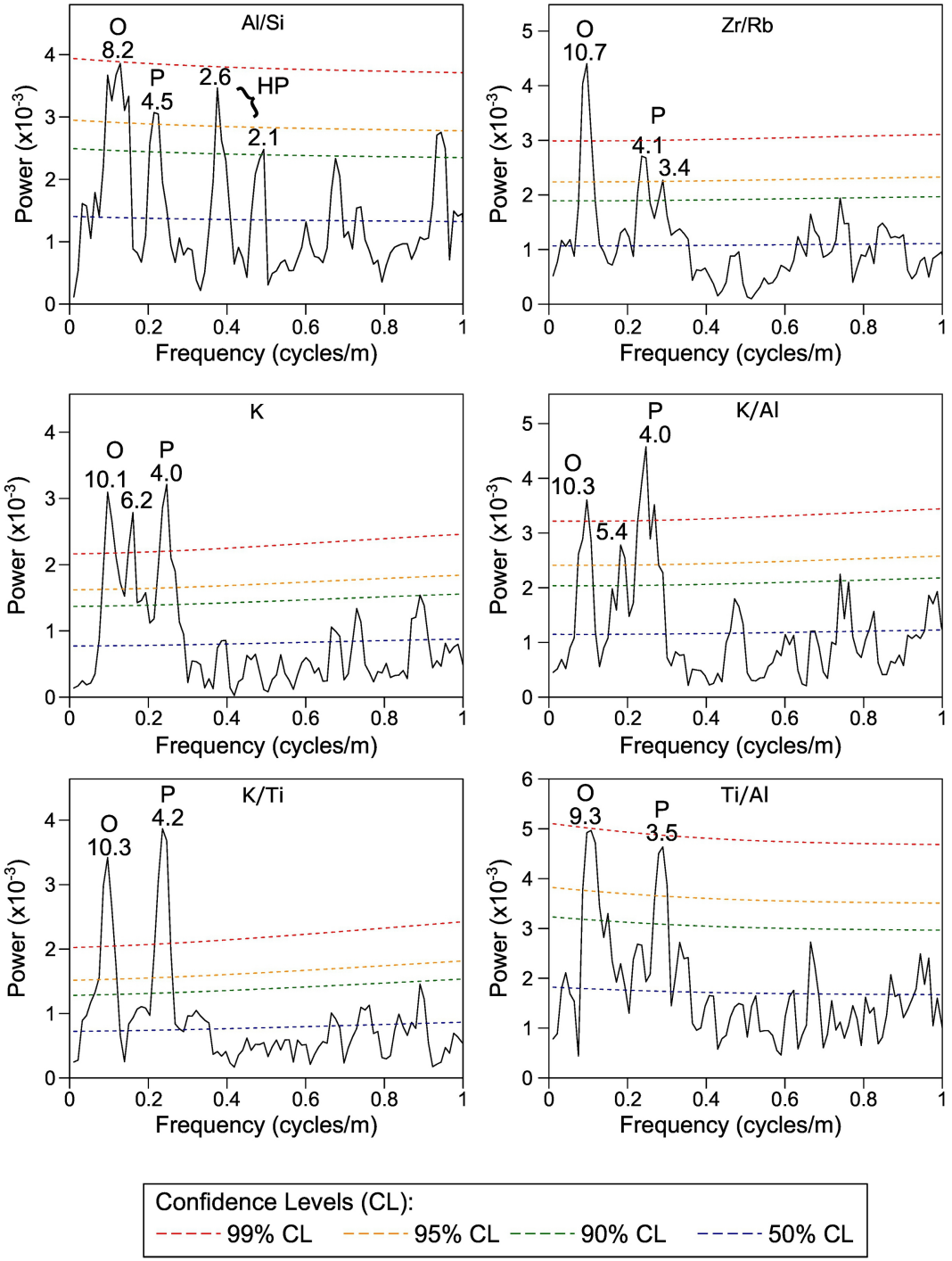
Al/Si
O
8.2
P
4.5
2.6
HP
2.1
Zr/Rb
O
10.7
P
4.1
3.4
K
O
10.1
6.2
P
4.0
K/Al
P
4.0
O
10.3
5.4
K/Ti
P
4.2
O
10.3
Ti/Al
O
9.3
P
3.5
Power (x10-3)
Frequency (cycles/m)
Confidence Levels (CL):
99% CL
95% CL
90% CL
50% CL

Figure 8

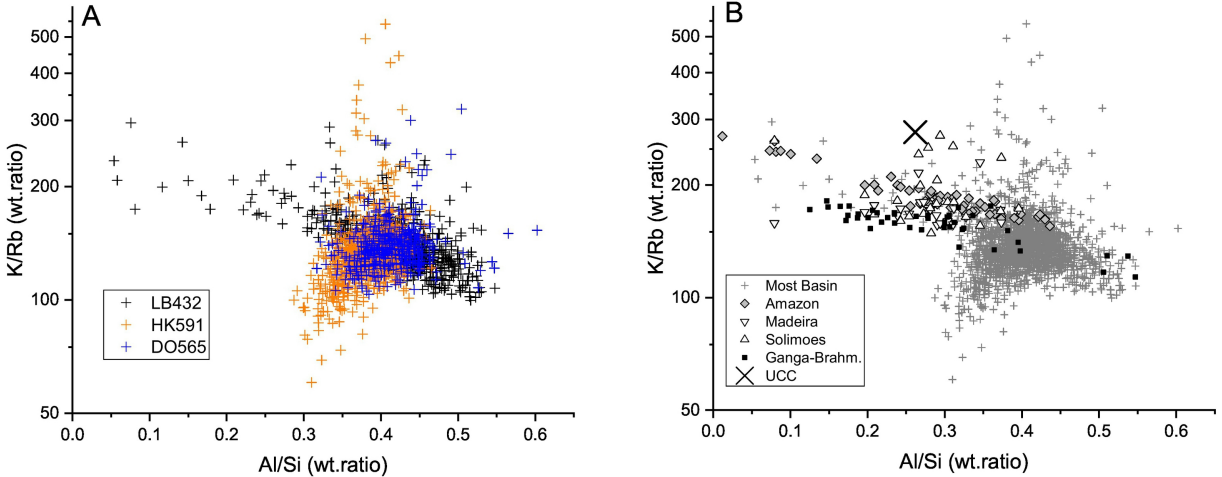
A
B
K/Rb (wt.ratio)
Al/Si (wt.ratio)
LB432
HK591
DO565
Most Basin
Amazon
Madeira
Solimoes
Ganga-Brahm.
UCC

Figure 9